Protein Science (1997), 6:1139–1147. Cambridge University Press. Printed in the USA.

Structural basis for the negative allostery between Ca^{2+}- and Mg^{2+}-binding in the intracellular Ca^{2+}-receptor calbindin D_{9k}

MARIA ANDERSSON,[1] ANDERS MALMENDAL,[2] SARA LINSE,[2] IANRIK IVARSSON,[1] STURE FORSÉN,[2] AND L. ANDERS SVENSSON[1]

[1]Department of Molecular Biophysics, Lund University, Center for Chemistry and Chemical Engineering, S-221 00 Lund, Sweden
[2]Department of Physical Chemistry 2, Lund University, Center for Chemistry and Chemical Engineering, S-221 00 Lund, Sweden

(RECEIVED December 26, 1996; ACCEPTED March 7, 1997)

Abstract

The three-dimensional structures of the magnesium- and manganese-bound forms of calbindin D_{9k} were determined to 1.6 Å and 1.9 Å resolution, respectively, using X-ray crystallography. These two structures are nearly identical but deviate significantly from both the calcium bound form and the metal ion-free (apo) form. The largest structural differences are seen in the C-terminal EF-hand, and involve changes in both metal ion coordination and helix packing. The N-terminal calcium binding site is not occupied by any metal ion in the magnesium and manganese structures, and shows little structural deviation from the apo and calcium bound forms. ^{1}H-NMR and UV spectroscopic studies at physiological ion concentrations show that the C-terminal site of the protein is significantly populated by magnesium at resting cell calcium levels, and that there is a negative allosteric interaction between magnesium and calcium binding. Calcium binding was found to occur with positive cooperativity at physiological magnesium concentration.

Keywords: allosteric interaction; calcium-binding protein; cooperativity; EF-hand protein; magnesium binding; nuclear magnetic resonance; X-ray crystallography

Magnesium is an essential element with structural and catalytic functions. Mg^{2+} is the most abundant divalent metal ion within cells, and the free Mg^{2+} concentration in the cytosol of eukaryotic cells remains nearly constant at about $0.5–2.0 \times 10^{-3}$ M (Ebel & Gunther, 1980). It is an important cofactor of enzymes that catalyse reactions underlying transcription, translation, and replication of nucleic acids (Black & Cowan, 1996a), and it regulates the activity of enzymes in major metabolic pathways such as glycolysis, amino acid synthesis, and photosynthesis (Black & Cowan, 1996b). The Mg^{2+} ion is also a potent competitor for the metal ion binding sites in intracellular proteins that regulate cellular processes in response to transient increases in the free Ca^{2+} concentration. These proteins belong to the calmodulin superfamily of EF-hand proteins (Nakayama et al., 1992), which also contain a number of proteins involved in buffering and trans-cellular transport of Ca^{2+} ions. In the resting cell, the free Ca^{2+} concentration is approximately 10^{-7} M, but it may transiently reach levels of 10^{-6} to 10^{-5} M as a result of a hormonal stimulation of a plasma membrane receptor. Although EF-hand proteins discriminate strongly against other divalent cations than Ca^{2+}, the high cytosolic Mg^{2+} concentration implies that many EF-sites are occupied by Mg^{2+} in a resting cell.

The intracellular calcium binding proteins sense and respond to changes in the free Ca^{2+} concentration between 0.1 and 10 μM on top of the mM Mg^{2+} background. The Ca^{2+} ion is bound in the loop region of the 29-residue long helix-loop-helix motif, "the EF hand" (Kretsinger & Nockolds, 1973). These motifs (or "subdomains") frequently appear in pairs or within larger domains and cooperative Ca^{2+} binding has been demonstrated in a considerable number of systems. The affinity for calcium is in many cases $10^2–10^4$-fold higher than for magnesium. In broad terms, the specificity is accomplished by taking advantage of the larger ionic radius of calcium and its less stringent demands on the number (often 7–8) and geometry of coordinating oxygen ligands. The smaller magnesium ion strongly prefers a sixfold coordination in an octahedral symmetry (Williams, 1976; Falke et al., 1994). Another important contribution to the higher Ca^{2+} affinity comes from the interactions with solvating water molecules being different for the respective free ions.

Hardly any details are presently known about the three-dimensional structures and other biophysical properties of the Mg^{2+} bound forms of EF-hand proteins. In order to provide a background for a rational explanation of biochemical observations we have undertaken a study of the crystal structure of the small glob-

Reprint requests to: Sara Linse, Physical Chemistry 2, Lund University, Chemical Centre, P.O. Box 124, S-221 00 Lund, Sweden; e-mail: sara@bor.fkem2.lth.se.

ular protein calbindin D_{9k} in the presence of Mg^{2+}. Further, ^{1}H-NMR studies and affinity measurements were undertaken. Calbindin D_{9k} is present in the small intestine at the site of Ca^{2+} and Mg^{2+} uptake, as well as in placenta, teeth, and bone (Christakos et al., 1989). The protein contains two EF-hands and binds two Ca^{2+}-ions with positive cooperativity and has long been thought/implied to take part in transcellular Ca^{2+} transport (Christakos et al., 1989; Walters et al., 1990). A recent study suggests that it also is involved in the active Mg^{2+} absorption in the intestine (Hemmingsen et al., 1996). Calbindin D_{9k} may thus be one of the components responsible for the close relation between calcium and magnesium metabolism, and the structure presented here could help explain its ability to function as a transporter for both types of ions. Within the superfamily of EF-hand proteins, calbindin D_{9k} belongs to the S100 proteins, which are a group of proteins with important functions in the regulation of the cell cycle (Schäfer & Heizmann, 1996). A common feature of these proteins is that one of the two EF-hands has a variant loop fold which, to a larger extent than normal, uses backbone carbonyl oxygens to coordinate the calcium ion (Szebenyi & Moffat, 1986; Svensson et al., 1992). Calbindin D_{9k} is an atypical member of this group, being a monomer in solution (Kördel et al., 1993; Akke et al., 1995; Skelton et al., 1995), whereas the NMR-derived structures of S100A6 (also called calcyclin; Potts et al., 1996), and S100B (Drohat et al., 1996) show that these proteins are homo-dimeric. Unlike the regulatory calmodulin proteins, calbindin D_{9k} undergoes only minor structural changes upon calcium binding.

Results and discussion

Description of the structure

The structure of recombinant bovine calbindin D_{9k} in its magnesium loaded state was determined using X-ray crystallography. Initial attempts to solve the structure by molecular replacement using the coordinates for either the calcium-loaded (Szebenyi & Moffat 1986; Svensson et al., 1992) or the ion-free state (Skelton et al., 1995) failed. Instead, the structure was solved to a resolution of 1.6 Å by multiple isomorphous replacement technique using the manganese loaded form of calbindin D_{9k} and a trimethyl-lead acetate derivative for phasing. The Mg^{2+} and Mn^{2+} containing crystal structures belong to the same space group and have a virtually identical structure. The root-mean-square deviation (RMSD) of 75 Cα atom pairs is only 0.1 Å. To further verify structural rearrangements in solution the ^{1}H-NMR chemical shifts for $(Mg^{2+})_1$ calbindin D_{9k} (Mg_1 calbindin) were partially assigned, and key NOE-contacts were identified.

Mg^{2+}-bound calbindin D_{9k} is a four-helix bundle formed from two EF-hand subdomains as outlined in Figure 1. The N-terminal EF-hand comprises helix I (residues 2–14), helix II (24–35), and metal binding loop I (14–27), while the C-terminal EF-hand comprises helix III (45–54), helix IV (62–73), and the metal binding loop II (54–65). The loops are positioned at the same end of the bundle and interact via a short β-type structure. Residues 36–44 form a linker region, connecting the two EF-hands.

Only one metal ion is observed in the magnesium and the manganese crystal structures, respectively. In both cases the metal ion is bound to the C-terminal *regular* EF-hand (site II). The N-terminal *pseudo* EF-hand (site I) is not occupied by any metal ion in these structures, in accordance with the very low Mg^{2+} affinity of this site, as measured by CD spectroscopy in solution (cf. Table 4).

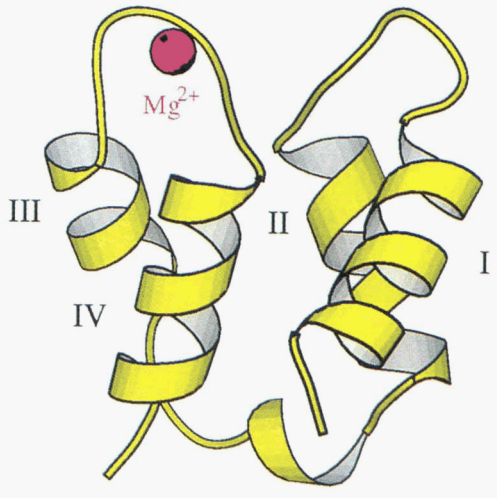

Fig. 1. Mg_1-calbindin D_{9k} with the *regular*, C-terminal EF-hand occupied by Mg^{2+} while the *pseudo*, N-terminal EF-hand contains no metal ion. The helices are numbered I, II, II, and IV, beginning from the N-terminus. (Figure generated with the Molscript program; Kraulis, 1991.)

This suggests that the N-terminal EF-hand has an extraordinary selectivity for calcium over the smaller magnesium and manganese ions, whereas the C-terminal EF-hand binds all three ions, although the calcium affinity is by far the highest. Site I is also selective against larger ions like lanthanide ions where binding is either not observed or more than 10^5-fold weaker than binding of Ca^{2+} ions (Hofmann et al., 1988). These lanthanide ions bind to site II with affinities within only one or two orders of magnitude from the Ca^{2+} affinity. The divalent cadmium ion has a similar ionic radius but different coordination geometry preferences from the calcium ion and bind to both sites in a sequential manner with site II being filled first (Vogel et al., 1985; Akke et al., 1991). The reason for the higher specificity for Ca^{2+} of the *pseudo* EF-hand loop might be the larger number of ligating backbone carbonyl oxygens. This *pseudo* EF-hand has four ligating carbonyl oxygen compared to one in a *regular* EF-hand. If ions with differing radius should be bound, this would lead to considerable rearrangement of the main chain to facilitate good coordination geometry.

The N-terminal EF-hand

The N-terminal calcium binding loop contains no metal ion in either Mg_1- or Mn_1-calbindin. During refinement a spherical electron density of about the size of a water molecule did emerge in the middle of the loop. A water molecule was inserted during refinement and the molecule obtained a temperature factor of 27.3 Å^2, similar to the values observed for the surrounding amino acids. The normal Ca^{2+} binding ligands, the carbonyl oxygens of Ala 14, Glu 17, Asp 19, and Gln 22, and one carboxyl oxygen of Glu 27, are at hydrogen bonding distance to the central atom (ranging between 2.5 and 3.07 Å, Table 1) in Mg_1-calbindin. The bond distances, donor/acceptor possibilities (all coordinating residues are probably acting as acceptors at pH 6.4), and the B-factors, suggest that the N-terminal EF-hand is occupied by a hydrogen bonded ammonium ion present in the crystallization matrix. As a consequence of the missing stabilizing metal ion, large thermal mobilities are observed in the loop region (Fig. 2a).

All of the residues in helix I are visible in the electron density with the exception of the first residue, a methionine (Met 0),

Table 1. *Ion-ligand distances for $(Mg^{2+})_1$, $(Mn^{2+})_1$, and $(Ca^{2+})_2$ states of calbindin D_{9k}*[a]

Loop I Residue	Atom	Ligand-ion distances (Å) Mg_1-form NH_4^+	Mn_1-form NH_4^+	Ca_2-form Ca^{2+}
Ala 14	O	3.07	3.24	2.33
Glu 17	O	2.52	2.56	2.47
Asp 19	O	2.71	3.03	2.25
Gln 22	O	2.68	2.92	2.36
Glu 27	Oε1	3.06	2.92	2.60
Glu 27	Oε2	3.35	3.16	2.42
Loop II residue	**Atom**	**Ligand-ion distances (Å) Mg_1-form Mg^{2+}**	**Mn_1-form Mn^{2+}**	**Ca_2-form Ca^{2+}**
Asp 54	Oδ	2.06	2.06	2.41
Asn 56	Oδ	2.05	2.19	2.34
Asp 58	Oδ	2.11	2.15	2.39
Glu 60	O	1.99	2.00	2.39
Glu 65	Oε1			2.54
Glu 65	Oε2			2.54
Wat 1	O	2.10	2.12	2.54
Wat 2	O	1.96	2.12	

[a]Distances between coordinating/hydrogen bonding atoms and ions in loop I and loop II of Mg_1, Mn_1, and Ca_2 forms (Svensson et al., 1992) of calbindin D_{9k}.

introduced in the expression stage. Helix II is also highly ordered. Helix I and helix II are connected via hydrogen bonds from Tyr 13 Oη and Lys 12 Nε to Glu 35 Oε1 (3.16 and 3.15 Å).

C-terminal EF-hand

In contrast to loop I, loop II is an archetypal 12 residue EF-hand loop. The Mg^{2+} ion in loop II is coordinated by six oxygen atoms, and the average Mg^{2+} to oxygen distance is 2.04 Å (Fig. 3a and Table 1). Three side chain oxygens (Asp 54 Oδ1, Asn 56 Oδ, and Asp 58 Oδ1), one carbonyl oxygen (Glu 60), and two water molecules function as ligands to the Mg^{2+} ion and form a perfect octahedron. One of the Mg^{2+} coordinating water molecules (Wat 1) is hydrogen bonded to the side chains of Gln 22 (2.59 Å Oε), Asp 58 (2.79 Å Oδ2) and Asn 56 (3.06 Å Nδ). The other Mg^{2+} coordinating water molecule (Wat 2) is hydrogen bonded by the side chain of Glu 65 Oε1 and by the C-terminal carboxyl group of a symmetry related molecule (2.59 Å and 2.64 Å, respectively). The coordinating water molecules are strongly bound, which is seen by the low B-values, which are on the same level as for the Mg^{2+} ion, 20 $Å^2$. The side chain oxygens of Glu 65 further make hydrogen bonds to the side chain of Ser 62 (2.63 Å) and to the main chain of Lys 55 (3.19 Å).

Helix III is well determined in the crystal structure and starts at Ser 44. It has an N-terminal helix capping hydrogen bond between Ser 44 Oγ and Leu 47 N (3.17 Å) not present in the Ca^{2+} form, and has consecutive $(i, i+4)$ helix hydrogen bonding pattern until Asp 54. Further, Asp 54 uses one of the side chain carboxylate oxygens to ligate the Mg^{2+} ion in the site (Fig. 3a).

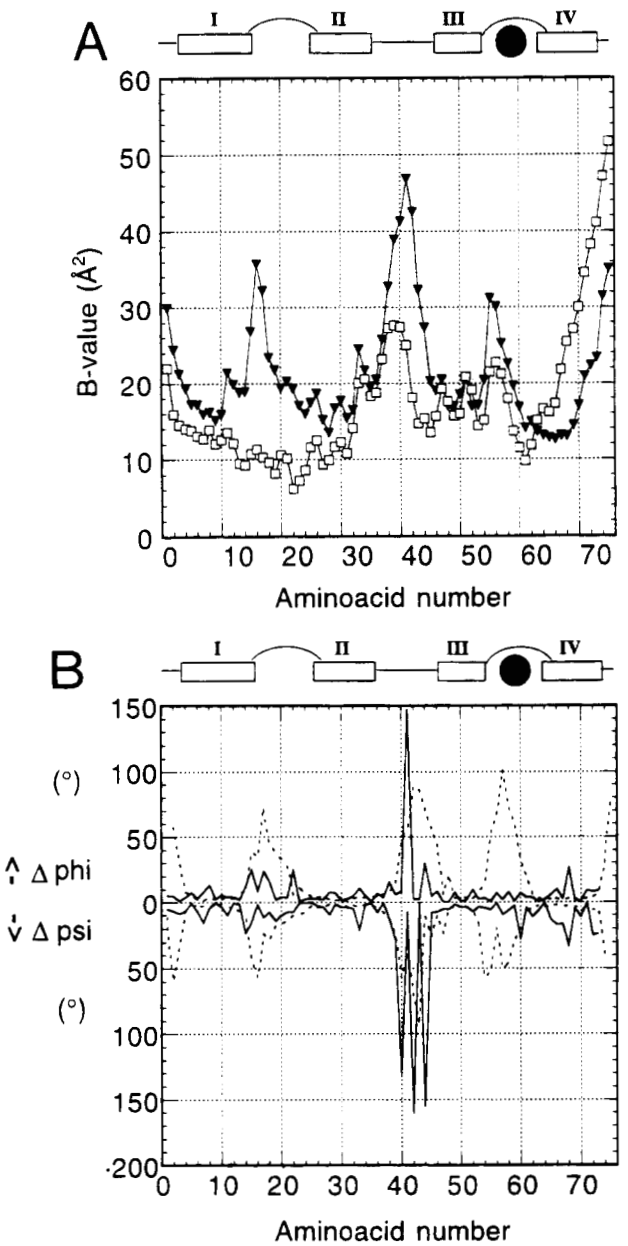

Fig. 2. A: Comparison of temperature factors for the main chain atoms of Mg_1- (down filled triangle) and Ca_2-calbindin (Svensson et al., 1992) (open square). Large B-values are observed in the linker region for both forms and in the unoccupied loop I of the Mg_1 form. Lower B-values are observed in helix IV for the Mg_1-compared to Ca_2-calbindin. **B:** Absolute differences in backbone dihedral angles between Mg_1 and Ca_2 (—), Mg_1 and ion-free (· · ·) forms of calbindin D_{9k}.

Helix IV of the Mg^{2+} form has a normal α-helix structure all the way from Ser 62 to Val 70. For the remaining five residues the hydrogen bonding pattern is a mixture of α-helix and 3_{10} helix.

Connections between the EF-hand subdomains

The two EF-hands are covalently connected via the linker region. In addition, there is a large number of non-covalent connections through extensive interactions within the hydrophobic core and

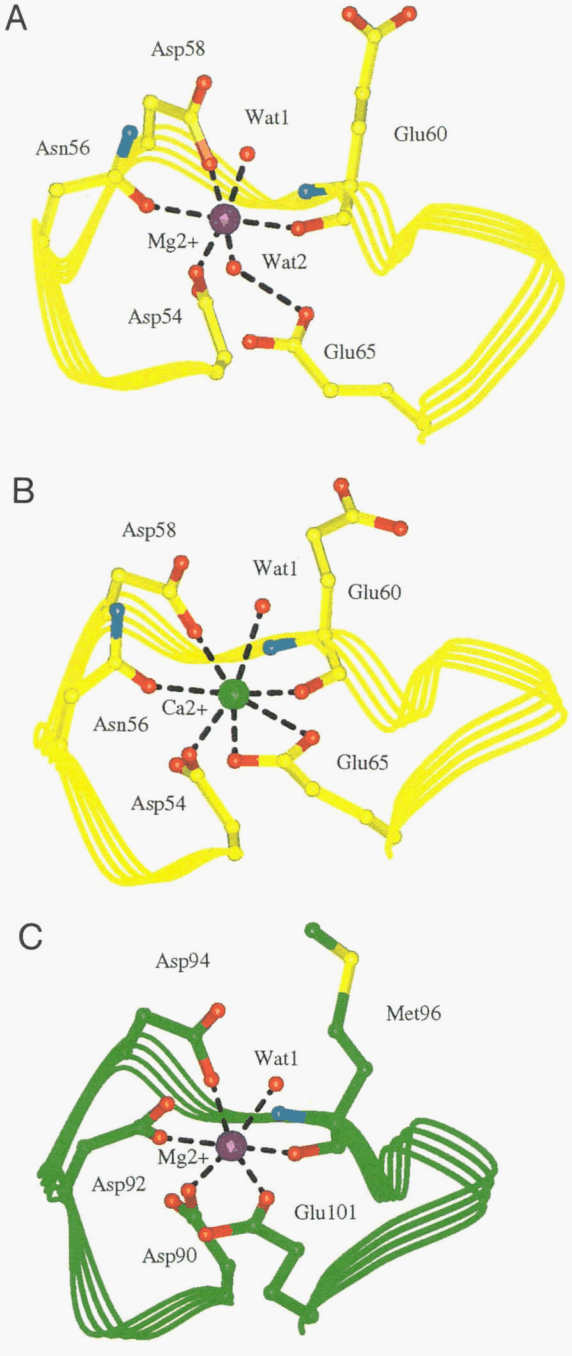

Fig. 3. Coordination of Mg^{2+} and Ca^{2+} in calbindin D_{9k} and parvalbumin. **A:** Coordination of Mg^{2+} (violet) in loop II of calbindin D_{9k}. **B:** Coordination of Ca^{2+} (green) in loop II of calbindin D_{9k} (Svensson et al., 1992). **C:** Coordination of Mg^{2+} (violet) in one of the C-terminal EF-hand of CaMgMg-parvalbumin (Declercq et al., 1991). The backbones of the loops are indicated as ribbon, whereas the essential side chains and backbone are shown as a ball-and-stick model.

hydrogen bonds between hydrophilic groups on the two subdomains. The linker region is mobile as seen from the low electron density and the high temperature factors of the model (Fig. 2a). In addition, residual densities in the difference maps $F_{obs} - F_{calc}$ and $2F_{obs} - F_{calc}$ are found in the region of the linker. The residual densities probably originate from alternate positions of the linker, however, not with enough occupancy to be modeled. The N-terminal part of the linker region has a short stretch of 3_{10} helix between residue 36 and 40. There is no electron density for residues 42 and 43, but residues Lys 41, Gly 42, and Pro 43 are modeled as a loop leading over to helix III. A hydrogen bond between Lys 25 Nϵ and Asp 47 Oϵ1 connects helix II with helix III.

Between the two EF-hand loops there is a short stretch of antiparallel β-sheet involving amino acids 22–24 and 59–61. A single pair of hydrogen bonds seen between Leu 23 and Val 61 (2.95 and 3.01 Å) stabilizes the sheet.

Comparison to calcium loaded and ion-free calbindin D_{9k}

The tertiary fold of Mg^{2+}-bound calbindin D_{9k} is distinctly different from both the ion-free (Skelton et al., 1995) and calcium-loaded (Svensson et al., 1992) forms, and the RMSDs of backbone-heavy atoms are 2.34 ± 0.31 and 2.26 Å, respectively (Table 2). The internal structures of the helices do not change upon Mg^{2+} binding, whereas the ion binding loops and the linker region act as hinges, allowing the helices to pack in a more compact manner in the Mg_1 form (Tables 2, 3, Figs. 2b, 5, 6). The structure of the β-sheet between the ion binding loops is slightly perturbed, with longer hydrogen bonds in the Mg_1 form (2.95 and 3.01 Å) than in the Ca_2 form (2.76 and 2.83 Å). This might indicate a weaker interaction between the two loops in the Mg_1 state. The changes in $C\alpha$–$C\alpha$ distances induced by Mg^{2+} and Ca^{2+} binding to calbindin D_{9k} are shown in Figure 4.

Several features of the Mg^{2+} coordination in the C-terminal site are distinctly different from the coordination of the Ca^{2+} ion in the same site as seen in the crystal structures of Ca_2-calbindin D_{9k} (Szebenyi & Moffat, 1986; Svensson et al., 1992) (Fig. 3b). The coordination number is lower (six compared to seven for Ca^{2+}) and the average metal ion to oxygen distance is shorter (2.04 compared to 2.42 Å for Ca^{2+}) (Table 1). The bidentate calcium-ligating glutamate in the 12th position of the EF-hand loop is a highly conserved feature of EF-hand proteins. When cations with larger ionic radius, such as Cd^{2+} and Ca^{2+}, bind to loop II, Glu 65 reaches its target by extending helix IV from a normal (i, i + 4) helix to a mixture of α- and 3_{10}-helical structure (Kördel et al.,

Table 2. *Comparison to ion-free and calcium-loaded calbindin D_{9k}*

	RMSD versus $(Ca^{2+})_2$[b]		Average RMSD versus ion-free[c]	
Residues[a]	All atoms[d]	Backbone[e]	All atoms[d]	Backbone[e]
All	2.67	2.26	2.89 ± 0.31	2.34 ± 0.31
EF1	1.40	0.71	1.91 ± 0.20	1.02 ± 0.19
EF2	2.64	2.13	2.63 ± 0.35	2.18 ± 0.37
Loop I	1.42	0.80	1.98 ± 0.33	0.96 ± 0.23
Loop II	1.42	1.00	2.29 ± 0.52	1.48 ± 0.57
Linker	2.61	1.58	3.05 ± 0.48	2.13 ± 0.35

[a]Residues used for superpositioning: All: 1–75; EF1: 3–35; EF2: 46–73; Loop I: 14–27; Loop II: 54–65; Linker: 36–45.

[b]RMSD between the $(Mg^{2+})_1$ structure and the $(Ca^{2+})_2$ structure (Svensson et al., 1992) of calbindin D_{9k}.

[c]Average RMSD between the $(Mg^{2+})_1$ structure and the family of 33 ion-free structures (Skelton et al., 1995) of calbindin D_{9k}.

[d]All non-hydrogen atoms.

[e]Backbone N, $C\alpha$, and C atoms.

Table 3. *Interhelical angles of the $(Mg^{2+})_1$, ion-free and $(Ca^{2+})_2$ states of calbindin D_{9k}*[a]

Helix pair	$(Mg^{2+})_1$ (°)	Ion-free (°)	$(Ca^{2+})_2$ (°)
I–II	124	118 ± 3	126
I–III	96	117 ± 8	118
I–IV	113	121 ± 3	119
II–III	125	118 ± 6	110
II–IV	47	38 ± 4	33
III–IV	145	119 ± 8	122

[a]The interhelical angles of the $(Mg^{2+})_1$, ion-free (Skelton et al., 1995), and $(Ca^{2+})_2$ (Svensson et al., 1992) states of calbindin D_{9k} were calculated by a program generously provided by Dr. Ikura. The interhelical angles are defined such that parallel helices have an interhelical angle of 0°, while the interhelical angle for antiparallel helices will be 180°. The residues included in the helices are: (I) 3–13, (II) 25–35, (III) 46–54, and (IV) 63–72.

1993; Akke et al., 1995; Skelton et al., 1995) (Figs. 4, 5). In the Mg^{2+}-loaded form of calbindin D_{9k} a water molecule, Wat 2, is introduced between the Mg^{2+} ion and the Glu 65 side chain. The Mg^{2+} ion is situated 0.8 Å further out in the EF-hand loop, relative to the Ca^{2+} ion and away from Glu 65, when superimposing the 12 Cα atom pairs of the respective loop. Differently to the Ca_2-state, only the very end of helix IV exhibits H-bonding characteristics of a 3_{10} helix. The other ligating water molecule, Wat 1, is observed in both the Mg_1 and the Ca_2 calbindin and is stabilized by hydrogen bonds to the side chains of Gln 22 and Asp 58. The mobility of the Gln 22 side chain is low in Ca_2-calbindin (B = 9 Å^2), but high in Mg-calbindin (B = 40 Å^2). The loss of stabilization by Gln 22 is compensated by a hydrogen bond between Wat 1 and Asn 56 Nϵ, which is not present in the Ca_2 form.

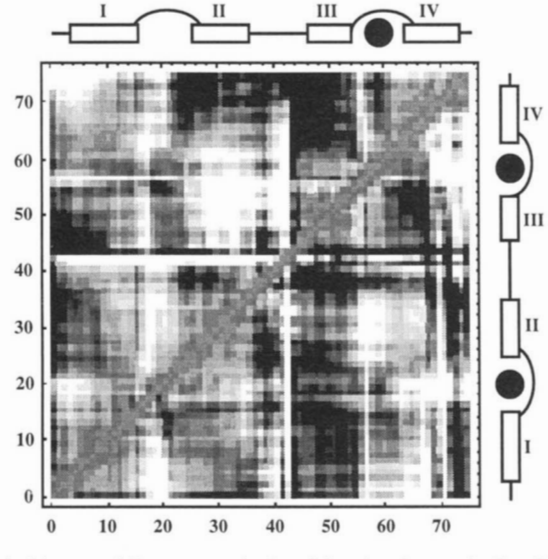

Fig. 4. Distance difference matrix describing the changes in Cα–Cα distances upon magnesium and calcium binding. The upper left half show the mean pairwise distance difference between all Cα atoms of the $(Mg^{2+})_1$ structure and the 33 structures of the ion-free state (Skelton et al., 1995) as a function of amino acid numbers. The lower right half show the mean pairwise distance difference between all Cα atoms of the $(Ca^{2+})_2$ structure (Svensson et al., 1992) and the 33 structures of the ion-free state. The graph is shaded so that distances that are unchanged by ion binding are gray, distances that become longer upon ion binding tend toward white, and distances that become shorter upon ion binding tend toward black.

The main differences relative to the Ca^{2+}-loaded and ion-free forms are found in the linker region between helix II and III and in the relative position of helix III and IV surrounding the Mg^{2+} occupied loop II (cf. Table 3, Figs. 4, 5b, 6b). The ligand geometry around the Mg^{2+} ion is accomplished by translating helix III about 2 Å towards loop II, compared to the ion-free and the Ca_2 forms. This enables helix IV to move in between helix II and III, decreasing the angle between helix III and IV by about 25° to a more compact form compared to Ca^{2+}-loaded and ion-free forms (Table 3, Figs. 4, 5b). The two solvent molecules connecting helix III with helix IV in the Ca_2 form are thus not present in the Mg_1 form. The more compact conformation with almost antiparallel helices is corroborated in solution by NOE contacts (Ile 73 HN–Leu 49 Hγ, Hδ). Detailed chemical shift analysis shows that in the Mg^{2+}-bound state, unlike the Ca_2-bound state, the packing of the side chains of Val 68, Leu 69, Val 70.,and Ile 73 in helix IV against the rest of the protein is similar to the ion-free state (Skelton et al., 1995; Wimberly et al., 1995). The side-chain packing is thus, despite the substantial rearrangement of helix IV, less affected by Mg^{2+} than Ca^{2+} binding. Most chemical shifts are more like those of the apo state except for the loop II region, where they are closer to those of Ca_2 calbindin.

The crystal structure of the Mg^{2+}-bound form of calbindin D_{9k} provides a possibility to analyze in detail the metal-ion free state of an EF-hand (site I). In contrast to the major changes of the Mg^{2+}-occupied EF-hand, only minor changes in tertiary structure relative to the calcium and apo forms are observed for the N-terminal EF-hand (Figs. 5a, 6a). The largest change in tertiary structure within this subdomain takes place in the loop, which is more open than the corresponding Ca^{2+} occupied loop. The RMSD of all backbone atoms in the N-terminal EF-hand between the Ca^{2+} and Mg^{2+} forms is 0.71 Å, while it is 0.80 for loop I alone (Table 2). Superposition of loop I for the Ca_2 form on the Mg_1 form reveals that the putative NH_4^+ ion resides within 0.65 Å of the relative position of the Ca^{2+} atom in Ca_2-calbindin. The ion binding loop retains most of its conformation, with four carbonyl oxygens pointing toward the center of site I making hydrogen bond to the NH_4^+ ion in the Mg_1 form in a similar fashion as they are coordinating Ca^{2+} in the Ca_2 form, however, displaying longer distances (Table 1). The three remaining Ca^{2+} ligands, the bidentate Glu 27 and a water molecule, are also in the proximity of the NH_4^+ ion. The water is hydrogen bonded to the side chain of Glu 60 reaching over from loop II in both the Mg_1 and the Ca_2 form.

The linker region between helix II and III show a large spatial difference in the Ca^{2+} and Mg^{2+} forms. The large differences in backbone dihedral angles between Mg_1-calbindin and Ca_2-calbindin (Fig. 2b) reveals that the linker is a hinge region, allowing the C-terminal EF-hand to pack differently when Mg^{2+} is bound.

Comparison to other Mg^{2+} binding EF-hand proteins

Very few structures of EF-hand proteins in their Mg^{2+} bound states are known. The Mg^{2+} coordination observed in calbindin D_{9k} is somewhat different from that in CaMgMg-parvalbumin (Declercq et al., 1991) (Fig. 3c) and myosin (Houdasse & Cohen, 1996). In these two structures, the side chain homologous to Glu 65 is a monodentate ligand to Mg^{2+}, as shown in Figure 3c. This type of Mg^{2+} coordination was proposed by Strynadka and

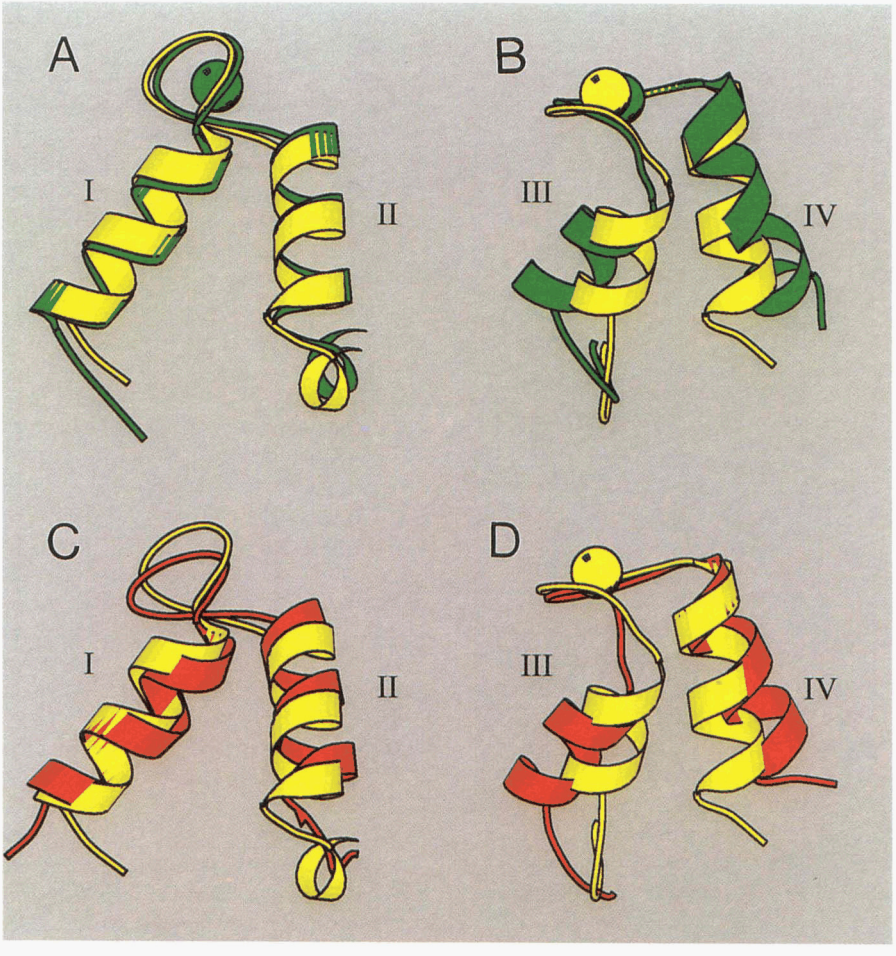

Fig. 5. Comparison of the tertiary structures of the Mg_1, Ca_2 (Svensson et al., 1992), and apo form (Skelton et al., 1995). **A:** The N-terminal EF-hand, residues 1–40, in the Mg_1 (yellow) and Ca_2 form (green). **B:** The C-terminal EF-hand, residues 41–75, in the Mg_1 (yellow) and Ca_2 form (green). **C:** The N-terminal EF-hand, residues 1–40, in the Mg_1 (yellow) and apo form (red). **D:** The C-terminal EF-hand, residues 41–75, in the Mg_1 (yellow) and apo form (red). The "hinge region" of the linker is included in panels B and D. The closer packing of helices III and IV in the C-terminal EF-hand upon Mg^{2+} binding are striking compared to the ion-free and the Ca_2 forms. The structures were overlaid using all Cα atoms and the figures were generated using the Molscript program (Kraulis, 1991).

James (1989) to be a general feature of Mg^{2+} binding to EF-hands. In the group of parvalbumin X-ray structures comprising the CaMgMg, Ca_2NH_4, Mn_2Mn, and Ca_2Mg forms (Declercq et al., 1991), no pair of structures have larger RMSD between Cα atoms than 0.54 Å compared to 2.26 Å found between the Mg_1 and Ca_2 forms of calbindin D_{9k}. The Mg^{2+} affinity of calbindin D_{9k} is 25 times lower than that of parvalbumin [K_D(calbindin) = 1 mM (cf. below), K_D(parvalbumin) = 41 μM, Eberhard & Erne, 1994], which may be a combined effect of larger conformational changes on Mg^{2+} binding to calbindin, and the larger number of water molecules in the coordination sphere.

Mg^{2+} binding characteristics

Themacroscopic Mg^{2+}- and Ca^{2+}-binding constants are summarized in Table 4. The values obtained at 150 mM KCl ($\log K_1$ = 3.0, $\log K_2$ = 0.9) show that the protein is capable of binding one magnesium ion under physiological salt conditions. At resting Ca^{2+} levels (0.5–2 mM Mg^{2+}) site II is thus 33–67% occupied by Mg^{2+}. Because the coordination of Mg^{2+} differs substantially from that of Ca^{2+}, one may ask if parallel Ca^{2+}/Mg^{2+} transport will occur with a majority of the protein molecules carrying one Ca^{2+}-ion and one Mg^{2+}-ion, or is the situation perhaps such that each protein molecule carries either two Ca^{2+} ions or one Mg^{2+} ion. It is, hence, of interest to investigate if there is any free-energy coupling between Mg^{2+} binding at site II and Ca^{2+} binding at site I. To address this question we have determined the Ca^{2+}-binding constants of calbindin D_{9k} in the presence of Mg^{2+}, monitored either by ^{1}H-NMR or by UV absorbance using a chromophoric Ca^{2+} chelator (5,5′Br_2-BAPTA) with high level of discrimination against Mg^{2+}. From the ^{1}H-NMR spectra we could estimate that at one equivalent of added Ca^{2+} most of the sample was either in the Mg_1 state, or in the Ca_2 state. A small fraction was in an intermediate form assumed to be the Ca_1Mg_1 state. This is indicative of positively cooperative Ca^{2+} binding. The UV titration confirms that Ca^{2+} binding occurs with positive cooperativity even in the presence of Mg^{2+} (Table 4). The reduction in overall affinity seen in the presence of 2 mM Mg^{2+} is primarily a consequence of a reduction of the first macroscopic Ca^{2+}-binding constant, and the apparent cooperativity of Ca^{2+} binding is, in fact, larger than in the absence of Mg^{2+}.

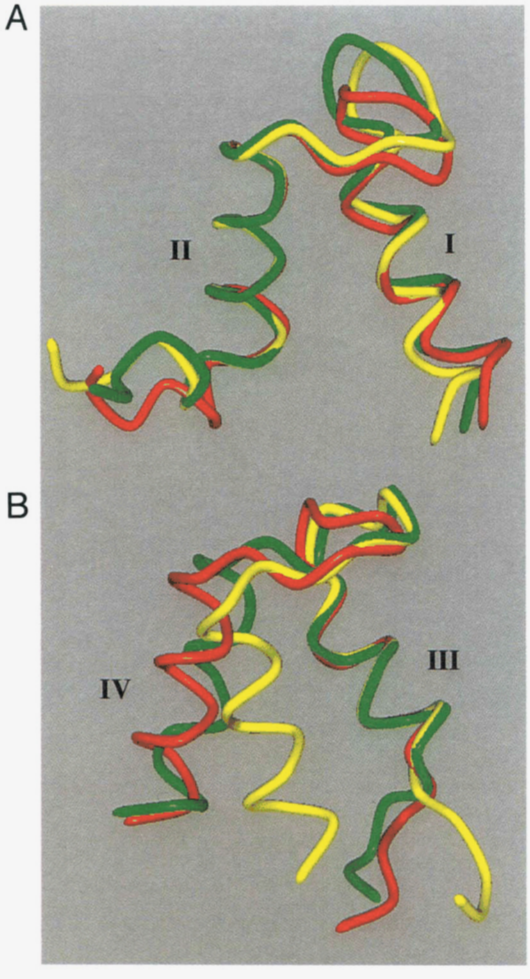

Fig. 6. Local effects of Mg^{2+} and Ca^{2+} binding on the N-terminal EF-hand and the linker relative to helix II (top) and on C-terminal EF-hand relative to helix III (bottom). The $(Mg^{2+})_1$ structure is shown in yellow, the ion-free structure (Skelton et al., 1995) in red, and the $(Ca^{2+})_2$ structure (Svensson et al., 1992) in green. Residues 2–43 are shown in the top panel and 41–74 in the bottom panel. The structures were overlaid using N, Cα, and C atoms of residues 25–35 (top) and residues 46–53 (bottom). The residues used in the overlay were chosen to monitor the importance of the Mg^{2+}-induced rearrangements.

The binding data in 0.15 M KCl in the absence and presence of Mg^{2+} (Table 4) can be used to estimate the free-energy coupling between Mg^{2+} binding to site II and Ca^{2+} binding at site I, using the additional information that $K_I \approx K_{II}$ in the absence of Mg^{2+} (Linse et al., 1991). The definitions of macroscopic and microscopic binding constants are given in Figure 7. In the absence of Mg^{2+}, $K_1 = 2 \times 10^6\ M^{-1}$, $K_2 = 3 \times 10^6\ M^{-1}$, $K_I \approx K_{II} = K_1/2 = 1 \times 10^6\ M^{-1}$; and $K_{I,II} \approx K_{II,I} = 6 \times 10^6\ M^{-1}$ (Linse et al., 1991). The apparent macroscopic Ca^{2+}-binding constants in the presence of 2 mM Mg^{2+} are $K_1 = 3 \times 10^5\ M^{-1}$ and $K_2 = 3 \times 10^6\ M^{-1}$. From the preserved value of K_2 we can estimate that Ca^{2+} binding at site I has reduced the Mg^{2+}-affinity at site II at least fivefold, otherwise competition with Mg^{2+} would reduce K_2 beyond the error limits.[1] The reduction in overall affinity, K_1K_2, could be a combination of competition with magnesium and negative allostery between Mg^{2+} and Ca^{2+} binding. An upper limit to the reduction in Ca^{2+} affinity at site I due to Mg^{2+} binding at site II is given by the case where the entire effect on K_1K_2 comes from the negative allostery, i.e., a factor of 6.3.

Thus, Mg^{2+} binding to site II reduces the Ca^{2+} affinity for site I about fivefold, and conversely, Ca^{2+} binding to site I leads to an about fivefold reduction in the Mg^{2+} binding constant of site II. A factor of 5 corresponds to an unfavorable free-energy coupling of 4 kJ·mol^{-1}. This suggests that calbindin D_{9k} can function as a transporter for both ions. When no Ca^{2+} is bound to the protein, the Mg^{2+} dissociation constant of site II is 1 mM, right in the physiological range. When Ca^{2+} binds to site I, the Mg^{2+} dissociation constant of site II increases to ca. 5 mM, which is above the physiological range, leading to the release of Mg^{2+} and an increase in apparent Ca^{2+} affinity. This enables Ca^{2+} binding to occur with positive cooperativity, despite the fact that magnesium "blocks" one calcium site, and calbindin D_{9k} can function as an efficient Ca^{2+} transporter or buffer at physiological Mg^{2+} concentrations.

The substantial differences in the Mg^{2+}- and Ca^{2+}-induced structural changes are likely to be a main cause of the unfavorable free-energy coupling between Mg^{2+} and Ca^{2+} binding. Although the structural changes in EF-hand I on Ca^{2+} binding to site I are minor, these changes are accompanied by structural rearrangements of EF-hand II, incompatible with the Mg^{2+} form and thus switching the conformation of the C-terminal half of the molecule toward the Ca_2 state (Wimberly et al., 1995).

Conclusions

The crystal structure of Mg^{2+}-bound calbindin D_{9k} shows that the structural changes accompanying Mg^{2+} binding are quite different from the structural changes observed on Ca^{2+} binding. As a consequence, Ca^{2+} and Mg^{2+} binding show mutual negative allostery,

[1] $K_2^{app} = K_2/(1 + [Mg^{2+}]/K_D)$. If $K_D = 1$ mM, $\log K_2^{app} = \log K_2 - 0.05$. If $K_D = 5$ mM, $\log K_2^{app} = \log K_2 - 0.15$.

Table 4. *Macroscopic Mg^{2+} and Ca^{2+} binding constants of calbindin D_{9k}*[a]

	Mg^{2+} binding		Ca^{2+} binding	
Solution conditions	$\log K_1$	$\log K_2$	$\log K_1$	$\log K_2$
Low salt (<2 mM KCl)	4.6 ± 0.1[d]	2.7 ± 0.1[b]	8.2 ± 0.1[d]	8.6 ± 0.1[d]
High salt (150 mM KCl)	3.0 ± 0.1[c]	0.9 ± 0.3[b]	6.3 ± 0.1[d]	6.5 ± 0.1[d]
High salt (150 mM KCl, 2 mM Mg^{2+})	—	—	5.5 ± 0.1[d]	6.5 ± 0.1[d]
High salt (150 mM KCl, 10 mM Mg^{2+})	—	—	$\log K_1K_2 = 11.5 \pm 0.1$[d,e]	

[a]The macroscopic binding constants K_1 and K_2 (reported as $^{10}\log K_1$ and $^{10}\log K_2$) for Mg^{2+} and Ca^{2+}, respectively, were derived from metal ion titrations using [b]CD, [c], and [d] UV spectroscopy. [e]K_1 and K_2 could not be resolved to high accuracy.

while Ca^{2+} binding occurs with positive cooperativity. The binding constants for Mg^{2+} and Ca^{2+} and the free energy of interaction between the two binding sites are elegantly tuned to physiological conditions in mammalian cells. As a result, calbindin D_{9k} can function as a transporter of both Ca^{2+} and Mg^{2+}.

Our data also suggest that at physiological Mg^{2+} concentrations the sequence of events subsequent to a transient increase in intracellular Ca^{2+} concentration will be as follows. The initial resting state of calbindin D_{9k} will have the *pseudo* EF-hand (site I) empty and the *regular* EF-hand (site II) occupied by Mg^{2+}. At elevated Ca^{2+} concentrations site I will be filled by Ca^{2+}, resulting in the release of Mg^{2+} from site II followed by Ca^{2+} entry into this site.

Methods

Bovine calbindin D_{9k} was expressed and purified in *E. coli* (Johansson et al., 1990). Magnesium calbindin D_{9k} crystals were obtained by vapor diffusion in plastic petri dishes. The concentrations were 35 mg/mL calcium-free protein, 75% ammonium sulfate pH 6.4, and 40–120 mM magnesium chloride. Manganese calbindin D_{9k} crystals were grown under similar conditions, 35 mg/mL protein, 65% ammonium sulfate pH 5.6, and 600 mM manganese sulfate. The crystals were isomorphous and belonged to the tetragonal space group $P4_32_12_1$, ($a = b = 33.73$ Å, $c = 129.47$ Å). Data from the Mg_1 form were collected using a Siemens X1000 area detector system and a Rigaku rotating anode operating at 45 kV and 90 mA. Data from the Mn_1 form were collected using an Image plate detector (MAR Research system) and a Rigaku rotating anode. All data were processed using the XDS system (Kabsch, 1993). A heavy atom derivative of the Mg_1 form was produced by increasing the pH from 6.4 to 6.9 and adding trimethyl-lead acetate to a final concentration of 13 mM. The crystals were soaked for six weeks. The heavy atom positions were determined from manual interpretations of difference Patterson Fourier map calculations and confirmed by cross-difference Fourier transforms. Scaling and phasing of data together with map calculations were performed using the CCP4 program system (Collaborative Computational Project Number 4, 1994). The maps were fitted using the program O (Jones et al., 1991) and refinement were carried out using X-PLOR (Brünger, 1992). Seventy-three out of 76 amino acids have been fitted into the electron density. Electron density is missing for the first amino acid, Met 0, and for Gly 42 and Pro 43 in the linker region. The initial crystallographic *R*-factor after slow cool refinement was 33.6%, and R_{free} was 41.7%. *R* and R_{free} were 26.5 and 34.1, respectively, in the step before restrained individual temperature factor refinement (for further statistics, see Table 5). The separation between *R* and R_{free} is somewhat larger than could be expected for a high-resolution structure. This is probably due to uninterpreted residual electron densities, especially in the linker region, which is highly mobile. According to the PROCHECK program (Laskowski et al., 1993), the variations from ideality in bond properties lie within the expected ranges and more than 95% of the residues lie in the most favored regions of a Ramachandran plot. Final coordinates are deposited in the Brookhaven Data Bank (5icb for Mg^{2+} form and 6icb for the Mn^{2+} form).

Table 5. *Statistics of structure determination*

	$(Mg)_1$-calb[a]	$(Mn)_1$-calb[b]	Pb[c]
Resolution (Å)	1.6	1.9	2.5
Observed reflections	54,446	17,782	24,645
Unique reflections	11,090	6,482	2,736
Completeness (%)	87	95	94
Riso[d] (%)		12.1	22.9
Sites (#)	1	1	2
Phasing power[e]		1.52	2.24
Refinement			
Resolution	10.0–1.6	10.0–1.88	
R-factor[f]	0.195	0.190	
R-free[g]	0.285	0.258	
RMSD on bond lengths[h] (Å)	0.020	0.018	
RMSD on bond angles[h] (°)	1.91	1.91	
RMSD on dihedrals[h] (°)	21.6	21.3	
Number of water molecules	50	36	

[a](Mg1)-calb = $(Mg^{2+})_1$-calbindin D_{9k}.
[b](Mn)1-calb = $(Mn^{2+})_1$-calbindin D_{9k}.
[c]Trimethyl-leadacetate derivative.
[d]Riso = $\Sigma(|\mathbf{F}_{PH} - F_P|)/\Sigma\mathbf{F}_P$.
[e]Phasing power = $(\Sigma|\mathbf{F}_H|^2/\Sigma(|\mathbf{F}_{PH} + -\mathbf{F}_P| - |\mathbf{F}_H|)^2)^{1/2}$.
[f]*R*-factor = $\Sigma|\mathbf{F}_{obs} - \mathbf{F}_{calc}|/\Sigma\mathbf{F}_{obs}$, where $\mathbf{F}_{obs}$ = refined $\mathbf{F}_{obs}$, 90% of total $\mathbf{F}_{obs}$.
[g]*R*-free = $\Sigma|\mathbf{F}_{test} - \mathbf{F}_{calc}|/\Sigma\mathbf{F}_{obs}$, where $\mathbf{F}_{test}$ = 10% of total $\mathbf{F}_{obs}$ not used in refinement.
[h]The RMSDs for bond lengths, angles, and dihedrals from ideal stereochemical values.

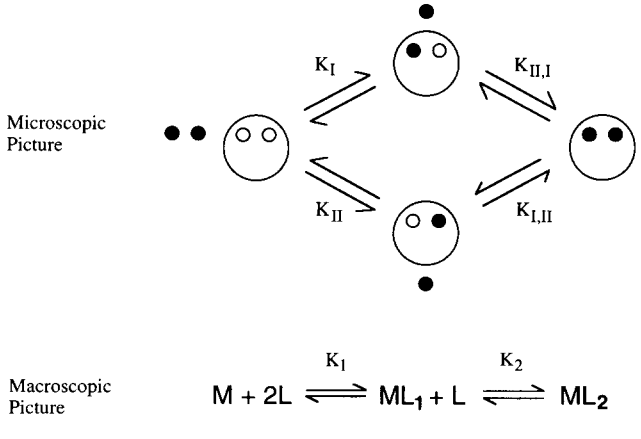

Fig. 7. Definition of microscopic (K_I, K_{II}, $K_{I,II}$, and $K_{II,I}$) and macroscopic (K_1 and K_2) binding constants for a protein with two biding sites I and II. $K_1 = K_I + K_{II}$. $K_1K_2 = K_IK_{II,I} = K_{II}K_{I,II}$.

^{1}H-NMR chemical shifts were assigned at 27 °C, pH 6 on a 4 mM calbindin D_{9k} sample[2] in 12 mM $MgCl_2$ from COSY, 2Q, TOCSY, and NOESY experiments using standard procedures (Chazin et al., 1988; Chazin & Wright, 1988). In the ^{1}H-NMR titrations, chemical shifts were followed using one-dimensional spectra.

The macroscopic binding constants K_1 and K_2 for Mg^{2+} and Ca^{2+}, respectively, were measured at 25 °C at low (<2 mM KCl) and high (150 mM KCl) salt concentrations. At low salt, the Mg^{2+}-binding constants were determined using UV spectroscopy to monitor the competition with quin 2 as described (Linse et al., 1991). The absorbance was recorded at 263 nm, where the absorbance of

[2]To avoid *cis-trans* isomerism around the Pro43-Ser44 bond the Pro43 → Gly mutant was used (Kördel et al., 1990).

the chelator changes significantly on Mg^{2+} binding while that of the protein remains constant. The Mg^{2+}-binding constant of quin 2, $\log K_{Mg} = 4.2$, was determined separately from Mg^{2+} titrations of quin 2 in the absence of protein. This value was then used to calculate the macroscopic Mg^{2+}-binding constants of the protein from the competition titration. The second macroscopic Mg^{2+}-binding constant was too low to be assessed with certainty from the competition titration and was instead measured from Mg^{2+} titrations monitored by near-UV CD (ellipticity at 277 nm, corresponding to the Tyr 13 signal) as described (Persson et al., 1989). At high salt, the Mg^{2+}-binding constants were derived from metal ion titrations of the protein using CD and NMR spectroscopy to monitor ion binding to the protein as described (Persson et al., 1989). The Ca^{2+}-binding constants in the presence of Mg^{2+} were derived using UV spectroscopy to monitor the competition with 5,5′Br_2BAPTA as described (Linse et al., 1991). The chelator 5,5′Br_2-BAPTA has a high level of discrimination against Mg^{2+} ($\log K_{Ca} = 5.65$; $\log K_{Mg} < 1$, at 0.15 M KCl).

Acknowledgments

This work was sponsored by the Swedish Natural Science Research Foundation (NFR Grant Numbers K 02545-300 and K 10178-300). The NMR spectrometer was purchased by generous support from the Wallenberg Foundation. A PhD Studentship sponsored by Pharmacia-Upjohn (for M.A.) is gratefully acknowledged. We thank Dr. Salam Al-Karadaghi for help with data collection. Dr. Walter J Chazin, Scripps, Dr. Anders Liljas, and Johan Evenäs for helpful discussions, and Eva Thulin for expression and purification of proteins.

References

Akke M, Forsén S, Chazin WJ. 1991. Molecular basis for co-operativity in Ca^{2+} binding to calbindin D_{9k}. ^{1}H NMR studies of $(Cd^{2+})_1$-bovine calbindin D_{9k}. *J Mol Biol 220*:173–189.

Akke M, Forsen S, Chazin WJ. 1995. Solution structure of $(Cd^{2+})_1$-calbindin D_{9k}. Comparisons to apo and $(Ca^{2+})_2$-calbindin D_{9k} reveal details of the structural changes of step-wise ion binding. *J Mol Bol 252*:102–121.

Black CB, Cowan JA. 1996a. Magnesium-dependent enzymes in nucleic acid biochemistry. In: Cowan JA, ed. *The biological chemistry of magnesium*. New York: VCH publishers Inc. pp 137–158.

Black CB, Cowan JA. 1996b. Magnesium-dependent enzymes in general metabolism. In: Cowan JA, ed. *The biological chemistry of magnesium*. New York: VCH Publishers Inc. pp 159–183.

Brünger AT. 1992. *X-PLOR (Version 3.1), A system for X-ray crystallography and NMR*. New Haven, Connecticut: Yale University Press.

Chazin WJ, Rance M, Wright PE. 1988. Complete assignment of the ^{1}H nuclear magnetic resonance spectrum of French bean plastocyanin. Application of an integrated approach to spin system identification in proteins. *J Mol Bol 202*:603–622.

Chazin WJ, Wright PE. 1988. Complete assignment of the ^{1}H nuclear magnetic resonance spectrum of French bean plastocyanin. Sequential resonance assignments, secondary structure and global fold. *J Mol Bol 202*:623–636.

Christakos S, Gabrielides C, Rhoten WB. 1989. Vitamin D-dependent calcium binding proteins: Chemistry, distribution, functional considerations, and molecular biology. *Endocr Rev 10*:3–26.

Collaborative Computational Project Number 4. 1994. *Acta Crystallogr D50*:760–763.

Declercq JP, Tinant B, Parello J, Rambaud J. 1991. Ionic interactions with parvalbumins: crystal structure determination of pike 4·10 parvalbumin in four different ionic environments. *J Mol Bol 220*:1017–1039.

Drohat AC, Amburgey JC, Abildgaand F, Starlich MR, Baldisseri D, Weber DJ. 1996. Solution structure of rat, apo-S100B ($\beta\beta$) as determined by NMR spectroscopy. *Biochemistry 35*:11577–11588.

Ebel H, Gunther T. 1980. Magnesium metabolism. *J Clin Chem Clin Biochem 18*:257–270.

Eberhard M, Erne P. 1994. Calcium and magnesium binding to rat parvalbumin. *FEBS Lett 222*:21–26.

Falke JJ, Drake SK, Hazard AL, Peersen OB. 1994. Molecular tuning of ion binding to calcium signalling proteins. *Q Rev Biophys 27*:219–290.

Hemmingsen C, Staun M, Olgaard K. 1996. Effects of magnesium on renal and intestinal calbindin-D. *Miner Electrolyte Metab 20*:265–273.

Hofmann T, Eng S, Lilja H, Drakenberg T, Vogel HJ, Forsen S. 1988. Site-site interactions in EF-hand calcium binding proteins *Eur J Biochem 172*:307–313.

Houdasse H, Cohen C. 1996. Strucure of the regulatory domain of scallop myosin at 2 Å resolution: Implications for regulation. *Structure 15*:21–32.

Johansson C, Brodin P, Grundström T, Thulin E, Forsén S, Drakenberg T. Biophysical studies of engineered mutant proteins based on calbindin D9k modified in the pseudo EF-hand. *Eur J Biochem 187*:455–460.

Jones TA, Zou JY, Cowan SW, Kjeldgaard M. 1991. Improved methods for building protein models in electron density maps and the location of errors in these models. *Acta Crystallogr A47*:110–119.

Kabsch W. 1993. Automatic processing of rotation diffraction data from crystals of initially unknown symmetry and cell constants. *J Appl Crystallogr 26*:795–800.

Kilby PM, Van Eldik LJ, Roberts GCK. 1996. The solution structure of the bovine S100B protein dimer in the calcium-free state. *Structure 4*:1041–1052.

Kördel J, Forsén S, Drakenberg T, Chazin WJ. 1990. Structural consequences of *cis-trans* isomerization in calbindin D_{9k}: ^{1}H NMR studies of the minor (*cis*-Pro-43) isoform and the Pro43Gly mutant. *Biochemistry 29*:4400–4409.

Kördel J, Skelton NJ, Akke M, Chazin WJ. 1993. High-resolution solution structure of calcium loaded calbindin D_{9k}. *J Mol Bol 231*:711–734.

Kraulis P. 1991. MOLSCRIPT: A program to produce both detailed and schematic plots of protein structures. *J Appl Crystallogr 24*:946–950.

Kretsinger RH, Nockolds CE. 1973. Carp muscle calcium binding protein. *J Biol Chem 248*:3313–3326.

Laskowski RA, MacArthur MW, Moss DS, Thornton JM. 1993. PROCHECK: A program to check the stereochemical quality of protein structures. *J Appl Crystallogr 26*:283–291.

Linse S, Johansson C, Brodin P, Grundström T, Drakenberg T, Forsén S. 1991. Electrostatic contributions to the binding of Ca^{2+} in calbindin D_{9k}. *Biochemistry 30*:154–162.

Nakayama S, Moncrief ND, Kretsinger RH. 1992. Evolution of EF-hand calcium-modulated proteins. II. Domain of several subfamilies have diverse evolutionary histories. *J Mol Evol 34*:416–448.

Persson E, Selander M, Linse S, Drakenberg T, Öhlin AK, Stenflo J. 1989. Calcium binding to the isolated β-hydroxyaspartic acid-containing epidermal growth factor-like domain of bovine factor X. *J Biol Chem 264*:16897–16904.

Potts BC, Smith J, Akke M, Macke TJ, Okazaki K, Hidaka H, Case DA, Chazin WJ. 1996. The structure of calcyclin reveals a novel homodimeric fold for S100 Ca^{2+}-binding proteins. *Nat Struct Biol 2*:790–796.

Schäfer BW, Heizmann CW. 1996. The S100 family of EF-hand calcium-binding proteins: Functions and pathology. *Trends Biochem Sci 21*:134–140.

Skelton NJ, Kordel J, Chazin WJ. 1995. Three-dimensional solution structure of apo calbindin D_{9k} determined by NMR spectroscopy. *J Mol Bol 249*:441–462.

Strynadka NC, James MN. 1989 Crystal structures of the helix-loop-helix calcium-binding proteins. *Annu Rev Biochem 58*:951–998.

Svensson LA, Thulin E, Forsen S. 1992. Proline *cis-trans* isomers in calbindin D_{9k} observed by X-ray crystallography. *J Mol Bol 223*:601–606.

Szebenyi DM, Moffat K. 1986. The refined structure of vitamin D-dependent calcium-binding protein from bovine intestine. *J Biol Chem 261*:8761–8777.

Vogel HJ, Drakenberg T, Forsen S, O'Neil JD, Hofmann T. 1985. Structural differences in the two calcium binding sites of the porcine intestinal calcium binding protein: A multinuclear NMR study. *Biochemistry 24*:3870–3876.

Walters JR, Howard A, Charpin MV, Gniecko KC, Brodin P, Thulin E, Forsén S. 1990. Stimulation of intestinal basolateral membrane calcium-pump activity by recombinant synthetic calbindin D_{9k} and specific mutants. *Biochem Biophys Res Commun 170*:603–608.

Williams RJP. 1976 *Calcium in biological systems*. Cambridge, UK: Cambridge University Press.

Wimberly B, Thulin E, Chazin WJ. 1995. Characterization of the N-terminal half-saturated state of calbindin D_{9k}: NMR studies of the N56A mutant. *Protein Sci 4*:1045–1055.